J|A|C|S COMMUNICATIONS

Published on Web 03/01/2006

Modulating Amyloid Self-Assembly and Fibril Morphology with Zn(II)

Jijun Dong,[§] Jacob E. Shokes,[†] Robert A. Scott,[†] and David G. Lynn*,[§]

Center for the Analysis of SupraMolecular Self-assemblies, Departments of Chemistry and Biology, Emory University, 1521 Dickey Drive, Atlanta, Georgia 30322, and Center for Metalloenzyme Studies and Department of Chemistry, University of Georgia, Athens, Georgia 30602-2556

Received September 8, 2005; E-mail: dlynn2@emory.edu

Interest in the molecular structure of amyloid fibrils originates both from their association with many devastating diseases and as systems for exploring the energetics of higher order protein folding and assembly. These fibril arrays are generally viewed as rich in β-sheets, of either parallel or antiparallel orientation.[1−5] However, the relative arrangement of the sheets within the fibril remains poorly constrained in the existing structure models,[4,6,7] as these sheet-to-sheet arrangements are mediated predominantly by side chain packing. We now extend the use of metal ions as probes of amyloid side chain packing in simple segments of the Aβ peptide of Alzheimer's disease. By restricting the possible metal binding sites, we show that Zn^{2+} can specifically control the rate of self-assembly and dramatically regulate amyloid morphology via distinct coordination environments.

The histidine dyad, His13 and His14, of Aβ is implicated in metal binding[8,9] and the metal-mediated toxicity of Aβ.[10−13] In a parallel, in-register β-sheet arrangement with sheet H-bonds oriented along the fibril axis (Figure 1a.),[3,4] the side chains of the His13 and His14 are spaced 5 Å apart along each surface of the β-sheets (Figure 1b). If the sheets are arrayed parallel to one another, the His13 and His14 side chains from different sheets are proximal, providing potential sites for Zn^{2+} chelation along the sheets (Figure 1b), between the sheets (Figure 1c), or both.[6]

Aβ(13−21), HHQKLVFFA, includes both the core segment, Aβ(17−21), known to be crucial for fibril formation,[14−18] and the metal binding dyad. To isolate His13/14 as the sole binding elements, the K16A peptide HHQALVFFA-NH_2, Aβ(13-21)K16A, was prepared. As shown in Figure 2a, Aβ(13−21)K16A develops β-sheet secondary structure within 49 h, showing an increased mean residue molar ellipticity (MRME) by circular dichroism (CD) at 197 and 212 nm. The development of β-sheet structure was further confirmed by FTIR, showing the appearance of the amide I absorbance at 1628 cm^{-1} (Figure S1a). TEM further established that Aβ(13-21)K16A assembles into fibrils (Fig. S1b), and these mature fibrils bind Congo red with the typical UV/vis absorption shift from 500 to 540 nm (Figure S1c).

Different Zn^{2+} concentrations dramatically altered both self-assembly kinetics and fibril morphology. The nucleation time was virtually eliminated with higher [Zn^{2+}] (Figure 2b), and this rapid assembly is accompanied by the formation of helical 5 ± 0.5 nm thick ribbons with widths of 30−50 nm (panel 1c, Figure 3). A mixture of fibrils and ribbons could be observed at low Zn^{2+} to peptide ratios (panel 1b, Figure 3), long homogeneous ribbons at 1:1 ratios (panel 1c, Figure 3), and with higher [Zn^{2+}], the ribbons are considerably shorter in length and tend to aggregate (panel 1d, Figure 3). When the ribbons from the 1:1 incubation were pelleted, washed, and analyzed, the Zn^{2+} to peptide ratio was 0.6−0.8 across three independent measurements.[19]

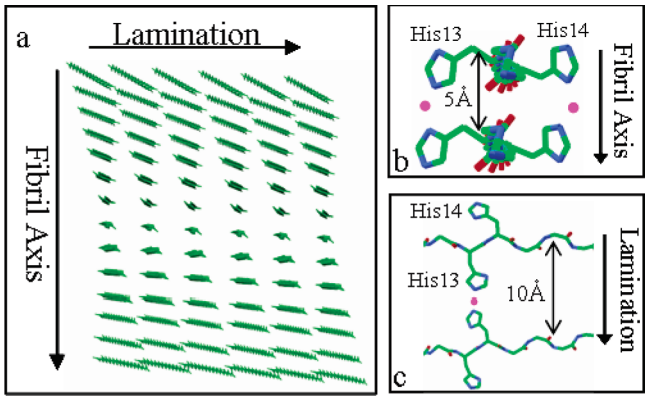

Figure 1. Metal binding sites predicted by the model of the Aβ(10−35) fibril. (a) The six-sheet laminated fibril with the backbone atoms shown. These fibrils are composed of β-strands, associating into β-sheet with hydrogen bond parallel to fibril long axis, while β-sheets laminate perpendicular to the fibril axis. The spacing between strands in the sheet and the mean distance between laminated sheets are ∼5 and ∼10 Å, respectively. (b) Potential zinc-binding site formed between two β-strands within a sheet, as viewed along the peptide backbones and perpendicular to the axis of fibril propagation. (c) Potential zinc-binding site formed between two strands of different sheets, as viewed down the axis of fibril propagation. Red, oxygen; blue, nitrogen; magenta, metal ion.

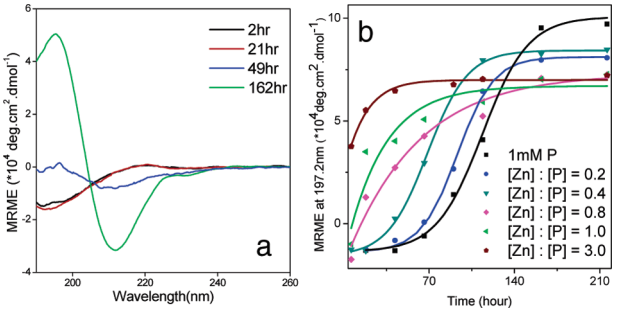

Figure 2. (a) CD spectra over time of 1 mM Aβ(13−21)K16A in 25 mM MES buffer at PH 5.6. (b) Mean residue molar ellipticity (MRME) at 197.2 nm as a function of time for 1 mM Aβ(13−21)K16A in the presence of different Zn^{2+}concentrations.

Wider 100−150 nm ribbons with variable twists form with longer incubation times (panels 2a,b, Figure 3). Some of the ribbons appear to coil and fuse to form tubular structures 200−300 nm in diameter (panels 2c,d, Figure 3). Therefore, Zn^{2+} reduces the nucleation time of self-assembly across the entire concentration range and transforms Aβ(13−21)K16A assembly into either fibrillar or ribbon/tubular morphology.[17]

Struck by the different morphologies accessible to Aβ(13−21)-K16A, we investigated the coordination environment of Zn^{2+} in the different assemblies by X-ray absorption spectroscopy (XAS). The soluble assembled metal−Aβ complexes were separated by centrifugation, and the fibers/ribbons were investigated either as

§ Emory University.
† University of Georgia.

10.1021/ja055973j CCC: $33.50

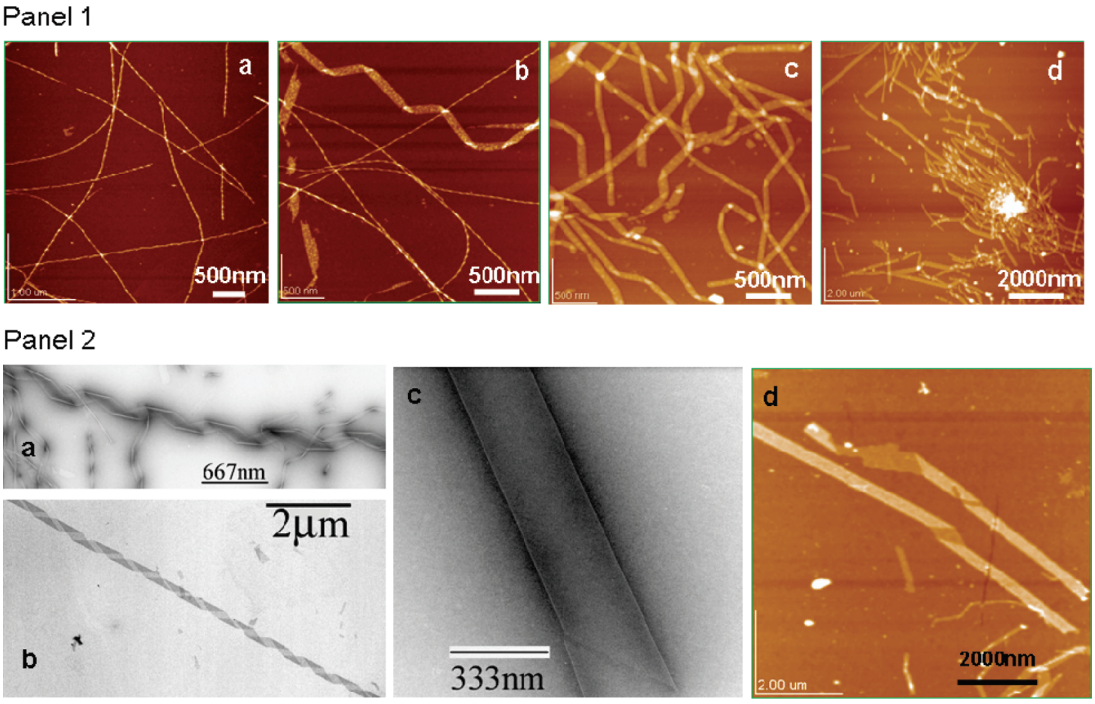

Figure 3. Panel 1: AFM for Aβ(13−21)K16A assembled with Zn^{2+} to peptide ratio of 0.2 (a), 0.8 (b), 1.0 (c), and 3.0 (d). Panel 2: TEM (a−c) and AFM (d) images of helical ribbons and nanotubes formed by Aβ(13−21)K16A assembled with a Zn^{2+} to peptide ratio of 1.0.

resuspended solutions or directly as hydrated pellets, both of which showed identical XAS spectra (Figure S2). The intensity and the position of the absorbance at the Zn *K*-edge region and EXAFS were consistent with four light elements (nitrogen or oxygen) in the coordination sphere of Zn^{2+} in the fibers/ribbons (Figure 4a), as well as the supernatant samples.[20,21] Curve fitting indicated either 3N(Im)/1O or 2N(Im)/2O atoms in the first Zn shell for the fiber/ribbon samples (Table S1), where N(Im) implies histidine imidazole coordination. The coincident appearances of the 3 and 4 Å peaks in the Fourier transform (Figure 4b) of the fiber/ribbon XAFS data (inset of Figure 4b) are diagnostic for two distinct imidazole ligands. The Zn^{2+} coordination environment in the fibers, $[Zn^{2+}]/[\text{peptide}] = 0.2$ and 0.6, are essentially identical; however, both the Zn *K*-edge absorption and EXAFS change when the Zn^{2+} to Aβ(13−21)K16A ratio reaches 1.0. The unusual relative intensities at 3 and 4 Å, which are typically equal in height as in the low $[Zn^{2+}]$ samples, could be the result of angular distortion of the imidazoles.[22] Therefore, the local Zn^{2+} coordination environment changes coincident with the change in morphology.

To test whether the difference in coordination environments observed in XAS and the associated morphologies may reflect different intra- and inter-sheet Zn^{2+} chelation, Ac-Aβ(13−21)H14A (Ac-HAQKLVFFA-NH_2) was investigated. As indicated in Figure 1, removal of His14 should eliminate inter-sheet metal binding while preserving coordination along the sheet surface. Ac-Aβ(13−21)-H14A formed fibrils in the absence of Zn^{2+}, showing the characteristic β-signature developing after 100 h (Figure 5a), coincident with the formation of typical long amyloid fibrils (Figure 5b). In the presence of 1 equiv of Zn^{2+}, the β signature developed more rapidly (Figure 5a); however, only homogeneous 10 nm diameter fibrils formed, at least up to a $[Zn^{2+}]/[\text{peptide}]$ ratio of 2.0 (Figure 5c). Assemblies formed from initial Zn^{2+} to peptide ratios of 1.0 gave a final ratio between 0.5 and 0.6, slightly lower than that of the Aβ(13−21)K16A peptide.[20]

The XAS results for the Zn^{2+}−fibrillar complex of Ac-Aβ(13−21)H14A were also consistent with a first Zn coordination shell of 3N(Im)/1O or 2N(Im)/2O atoms (Figure S3 and Table S1). The

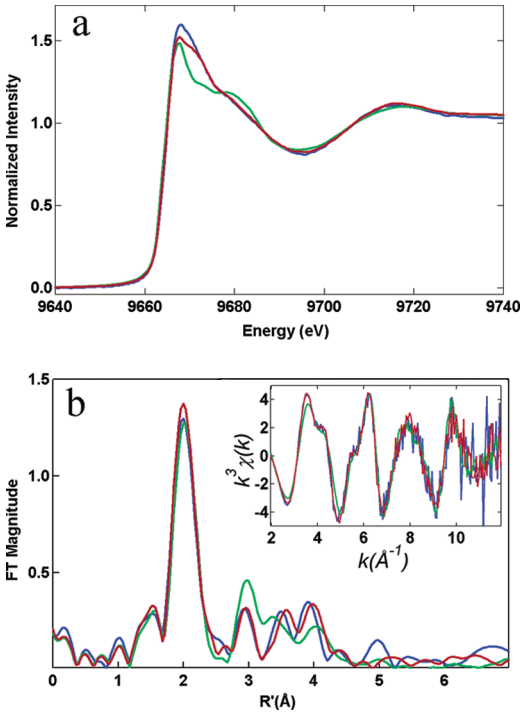

Figure 4. Zn *K*-edge X-ray absorption spectrum (a) and Fourier transforms (b) of the EXAFS (inset of b) for Zn^{2+} in Aβ(13−21)K16A assemblies formed with initial $[Zn^{2+}]/[A\beta(13-21)K16A] = 0.2$ (red), 0.6 (blue), and 1.0 (green). The data were collected at a temperature of 10 K, which was maintained by a continuous flow liquid helium cryostat. The averaged XAS data represent 10 scans, each of 21 min duration. EXAFSPAK software (www-ssrl.slac.stanford.edu/exafspak.html) was used for data reduction and analysis.

appearance of the 3 and 4 Å peaks in the Fourier transform of the EXAFS again were diagnostic for two imidazoles, consistent with two His13's on one face of the β-sheet chelating Zn^{2+} and similar to that seen for Aβ(13−21)K16A at low $[Zn^{2+}]$. Such intra-sheet His−Zn^{2+}−His chelation could stabilize side chain packing along

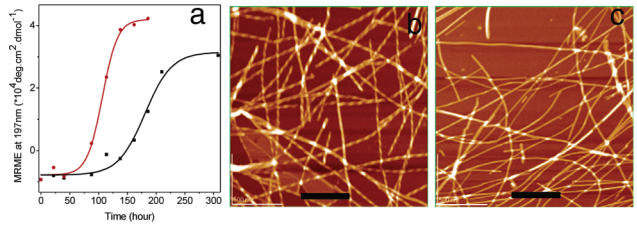

Figure 5. (a) Mean residue molar ellipticity (MRME) at 197 nm as a function of time for 2 mM Ac-Aβ(13−21)H14A (black) and in the presence of 2 mM Zn^{2+} (red). (b and c) AFM for Ac-Aβ(13−21)H14A (b) and in the presence of Zn^{2+} (c). Scale bar = 500 nm. For AFM, tapping mode analysis on a JEOL JSPM-4210 employed ultra-sharp noncontact silicon cantilevers with typical frequencies between 240 and 350 kHz.

the sheet, consistent with the acceleration of β-sheet growth. The intensity of the first-shell Fourier transform FT peaks around 2 Å in the Ac-Aβ(13−21)H14A fibrils was more intense than that in the Aβ(13−21)K16A assemblies, implying that Ac-Aβ(13−21)-H14A fibrils contain less heterogeneity and greater inherent local order (Figure S3b).

Transition metals have been implicated in amyloid fibril assembly for several years,[13,23,24] but their ability to alter fibril morphology has not been appreciated. By resolving a single binding site in the amyloid array and observing the metal directly, we have taken the first step to reveal how metal coordination may dictate amyloid assembly morphology. Although the other ligands that chelate Zn^{2+} in both Aβ(13−21)K16A and Ac-Aβ(13−21)H14A assemblies are not known, but must include the N-terminal amino group or the Lys and Gln side chains, our data revealed different His−Zn^{2+}−His chelation modes in metal-induced assemblies by these two short amyloid segments. Initial solid state NMR and isotope editing FTIR results reveal a parallel in-register β-sheet orientation in the assemblies of both peptides. Therefore in Ac-Aβ(13−21)H14A, the most plausible model is that His13 residues on two different peptides chelate the metal along the entire face of each β-sheet. In Aβ(13−21)K16A, where the His13/His14 dyad is present, distinct Zn^{2+} coordination can be accessed at elevated [Zn^{2+}], capturing the His residues between adjacent sheets to stabilize parallel sheet/sheet associations and the transition to the ribbon/tube morphology. These characteristic spectroscopic signatures can now be investigated in the full-length Aβ assemblies, allowing determination of the different coordination complexes in the more complex structures, creating probes for different metals, and revealing characteristic chemical reactivity that may be important for cellular toxicity. The emerging insight into the toxicity of these structures will undoubtedly be critical in providing models for developing therapeutic intervention strategies.

Clearly, these results demonstrate that differential control of conditions can modulate β-sheet growth and sheet/sheet packing and, hence, open the possibility of better constraining amyloid structure and the mechanism of amyloid self-assembly. The variety of self-assembled architectures achieved by modulating metal ion concentrations offers far greater morphological control and further raises the possibility of adapting such scaffolds for novel materials applications.

Acknowledgment. The XAS data were collected at the Stanford Synchrotron Radiation Laboratory, a national user facility operated by Stanford University on behalf of the U.S. Department of Energy, Office of Basic Energy Sciences. The SSRL Structural Molecular Biology Program is supported by the Department of Energy, Office of Biological and Environmental Research, and by the National Institutes of Health, National Center for Research Resources, and Biomedical Technology Program. We thank DOE ER15377 (D.G.L.) and NIH GM42025 (R.A.S.) for support, NSF (CHE-0131013) for CD instrumentation, Emory microscopy core laboratory for TEM, and C.L. Emerson for AFM instrumentation.

Supporting Information Available: Peptide synthesis, FTIR, TEM, Congo Red binding, and XAS analyses as well as the full citation for ref 11 are available. This material is available free of charge via the Internet at http://pubs.acs.org.

References

(1) Antzutkin, O. N.; Balbach, J. J.; Leapman, R. D.; Rizzo, N. W.; Reed, J.; Tycko, R. *Proc. Natl. Acad. Sci. U.S.A.* **2000**, *97*, 13045−13050.
(2) Balbach, J. J.; Ishii, Y.; Antzutkin, O. N.; Leapman, R. D.; Rizzo, N. W.; Dyda, F.; Reed, J.; Tycko, R. *Biochemistry* **2000**, *39*, 13748−13759.
(3) Benzinger, T. L. S.; Gregory, D. M.; Burkoth, T. S.; Miller-Auer, H.; Lynn, D. G.; Botto, R. E.; Meredith, S. C. *Proc. Natl. Acad. Sci. U.S.A.* **1998**, *95*, 13407−13412.
(4) Burkoth, T. S.; Benzinger, T. L. S.; Urban, V.; Morgan, D. M.; Gregory, D. M.; Thiyagarajan, P.; Botto, R. E.; Meredith, S. C.; Lynn, D. G. *J. Am. Chem. Soc.* **2000**, *122*, 7883−7889.
(5) Inouye, H.; Fraser, P. E.; Kirschner, D. A. *Biophys. J.* **1993**, *64*, 502−519.
(6) Morgan, D. M.; Dong, J. J.; Jacob, J.; Lu, K.; Apkarian, R. P.; Thiyagarajan, P.; Lynn, D. G. *J. Am. Chem. Soc.* **2002**, *124*, 12644−12645.
(7) Nelson, R.; Sawaya, M. R.; Balbirnie, M.; Madssen, A.; Riekel, C.; Grothe, R.; Eisenberg, D. *Nature* **2005**, *435*, 773−778.
(8) Miura, T.; Suzuki, K.; Kohata, N.; Takeuchi, H. *Biochemistry* **2000**, *39*, 7024−7031.
(9) Yang, D. S.; McLaurin, J.; Qin, K.; Westaway, D.; Fraser, P. E. *Eur. J. Biochem.* **2000**, *267*, 6692−6698.
(10) Cherny, R. A.; et al. *Neuron* **2001**, *30*, 665−676.
(11) Frederickson, C. J.; Bush, A. I. *Biometals* **2001**, *14*, 353−366.
(12) Huang, X. D.; Cuajungco, M. P.; Atwood, C. S.; Moir, R. D.; Tanzi, R. E.; Bush, A. I. *J. Nutr.* **2000**, *130*, 1488s−1492s.
(13) Jobling, M. F.; Huang, X. D.; Stewart, L. R.; Barnham, K. J.; Curtain, C.; Volitakis, I.; Perugini, M.; White, A. R.; Cherny, R. A.; Masters, C. L.; Barrow, C. J.; Collins, S. J.; Bush, A. I.; Cappai, R. *Biochemistry* **2001**, *40*, 8073−8084.
(14) Hilbich, C.; Kisters-Woike, B.; Reed, J.; Masters, C. L.; Beyreuther, K. *J. Mol. Biol.* **1992**, *228*, 460−473.
(15) Benzinger, T. L.; Gregory, D. M.; Burkoth, T. S.; Miller-Auer, H.; Lynn, D. G.; Botto, R. E.; Meredith, S. C. *Biochemistry* **2000**, *39*, 3491−3499.
(16) Gordon, D. J.; Balbach, J. J.; Tycko, R.; Meredith, S. C. *Biophys. J.* **2004**, *86*, 428−434.
(17) Lu, K.; Jacob, J.; Thiyagarajan, P.; Conticello, V. P.; Lynn, D. G. *J. Am. Chem. Soc.* **2003**, *125*, 6391−6393.
(18) Soreghan, B.; Kosmoski, J.; Glabe, C. *J. Biol. Chem.* **1994**, *269*, 28551−28554.
(19) Ribbon assemblies, formed from solutions with an initial Zn^{2+} to Aβ(13−21)K16A ratio of 1.0, were separated from nonaggregated peptides and free metal ions by centrifugation at 16 110*g* for 1 h, and the pellet was repeatedly washed with fresh MES buffer solution. The total Zn^{2+} in the suspended pellet solution was determined by Inductively Coupled Plasma Mass Spectrometry (ICP-MS) at the chemical analysis laboratory of the University of Georgia, and the peptide concentration was obtained from amino acid analysis (AAA) at Keck biotechnology resource laboratory at Yale University.
(20) Clark-Baldwin, K.; Tierney, D. L.; Govindaswamy, N.; Gruff, E. S.; Kim, C.; Berg, J.; Koch, S. A.; Penner-Hahn, J. E. *J. Am. Chem. Soc.* **1998**, *120*, 8401−8409.
(21) Jacquamet, L.; Aberdam, D.; Adrait, A.; Hazemann, J. L.; Latour, J. M.; Michaud-Soret, I. *Biochemistry* **1998**, *37*, 2564−2571.
(22) Ferreira, G. C.; Franco, R.; Mangravita, A.; George, G. N. *Biochemistry* **2002**, *41*, 4809−4818.
(23) Bush, A. I.; Pettingell, W. H.; Multhaup, G.; Paradis, M. D.; Vonsattel, J. P.; Gusella, J. F.; Beyreuther, K.; Masters, C. L.; Tanzi, R. E. *Science* **1994**, *265*, 1464−1467.
(24) Jones, C. E.; Abdelraheim, S. R.; Brown, D. R.; Viles, J. H. *J. Biol. Chem.* **2004**, *279*, 32018−32027.

JA055973J